jmp STATISTICAL DISCOVERY

The Relevance of Measurement Systems Analysis

A Procter & Gamble Case Study on MSA Methodology and Applications

DATE
OCTOBER 10 AND 12

TIME
16:00 CET, 10 am EST

CHRISTIAN NEU
Scientist
Procter & Gamble

JERRY FISH
Systems Engineer
JMP

JASON WIGGINS
Senior Systems Engineer
JMP

Register now

ADVANCED ENGINEERING MATERIALS
www.aem-journal.com

Controlling Degree of Inversion in $MgFe_2O_4$ Spinel Films Grown in External Magnetic Fields

*Hyeonkwon Lee, Ziyaad T. Aytuna, Aman Bhardwaj, Michael Wilhelm, Khan Lê, Benjamin May, David N. Mueller, and Sanjay Mathur**

Single-phase magnesium ferrite spinel films ($MgFe_2O_4$) were grown by magnetic field-assisted chemical vapor deposition (mfCVD) of a mixed-metal precursor compound, [$MgFe_2(O^tBu)_8$]. The formation of monophasic $MgFe_2O_4$ deposits as a function of the applied magnetic field strength ($B = 0.0$, 0.5, and 1.0 T) was investigated and confirmed by X-ray diffraction and photoelectron spectroscopy analyses. Thin film cross-sectional electron microscopic analysis (FIB-SEM) exhibited higher grain growth and densification in $MgFe_2O_4$ films obtained under the magnetic field influence when compared to spinel samples grown under zero-field conditions. Application of an external magnetic field of varying strengths during the chemical vapor deposition process resulted in a change in the light absorption properties and crystal orientation in the $MgFe_2O_4$ films, evident in the decreased photoabsorbance analyzed by the UV-Vis spectra and the decrease of intensity of the (400) peak in $MgFe_2O_4$ films grown under magnetic field. A comprehensive analysis of X-ray diffraction and X-ray magnetic circular dichroism (XMCD) results indicated a higher degree of inversion in $MgFe_2O_4$ deposits grown in an external magnetic field corroborated by a larger contribution of ligand field transitions of tetrahedrally coordinated Fe(III) centers affecting the visible light absorption of $MgFe_2O_4$ films.

1. Introduction

The class of spinel ferrites with general formula MFe_2O_4 (M = bivalent main group or transition metal cation) is of significant scientific and technological interests due to their tunable magnetoelectrical, photocatalytic, and photoelectrochemical properties. Given their ferromagnetic properties that can be modulated under applied magnetic fields, they find extensive applications in magnetic data storage, telecommunication, catalysis, and sensors.[1,2] Spinel structure is composed of anions forming face-centered-cubic (FCC) structure and two types of cations (M^{2+} and M^{3+}) occupying interstitial octahedral and tetrahedral sites in the FCC lattice.[3,4] A characteristic structural property of spinel ferrites is the cation disorder expressed as the degree of inversion, which manifests the exchange of M^{2+} cations from tetrahedral sites to the octahedral sites occupied by Fe^{3+} cations in the regular (normal) spinel. The degree of inversion in spinel ferrites largely depends on the synthesis conditions and is subject to the nature of precursors and processing conditions, and thus a broad range of cation distribution (between 0.1 and 0.9) has been reported.[5] Since spinel samples display different magnetic properties depending on whether they possess normal or inverse structures,[6,7] careful control over the synthesis conditions is crucial to establish a structure–property relationship in soft spinel ferrites. For example, normal and inverse spinel show different ion transport and stability undergoing lithiated and delithiated states.[3,8–10]

While spinel crystals such as $MgAl_2O_4$ found in nature generally exhibit a regular structure, the synthetic samples mostly exhibit a significant degree of inversion, possibly due to the faster kinetics of crystallization that is inhibitive for required cation exchange in the lattice. On the other hand, the formation of inverse spinel-like Fe_3O_4 in nature is favored with Fe^{2+} centers preferentially occupying the octahedral sites rather than the tetrahedral positions. The ferrimagnetic behavior and net magnetic moment in ferrite spinels result from the antiferromagnetic coupling between Fe^{3+} ions at octahedral and tetrahedral sites through the electronic orbitals of bridging oxygen centers (**Figure 1**).[11,12] In previous studies, we have shown that judicious changes in synthesis parameters such as choice of precursor, precursor flux, substrate, and precursor temperature, and duration can significantly affect the characteristics of the target material.[13–15] In the context of molecule-based materials synthesis, Mathur et al. reported on the deposition of $MgAl_2O_4$ spinel structure from three different Mg–Al precursors, namely [$MgAl_2(O^iPr)_8$], [$MgAl_2(O^tBu)_8$], and [$MgAl_2H_4(O^tBu)_4$].[16] The slight changes in the chemical configuration of the three precursors were shown to predominantly influence the vapor pressure,

H. Lee, Z. T. Aytuna, A. Bhardwaj, M. Wilhelm, K. Lê, S. Mathur
Institute of Inorganic Chemistry
University of Cologne
Greinstr. 6, 50939 Cologne, Germany
E-mail: sanjay.mathur@uni-koeln.de

B. May, D. N. Mueller
PGI-6
Research Centre
Juelich GmbH
Leo-Brandt-Str., 52428 Juelich, Germany

DOI: 10.1002/adem.202300021

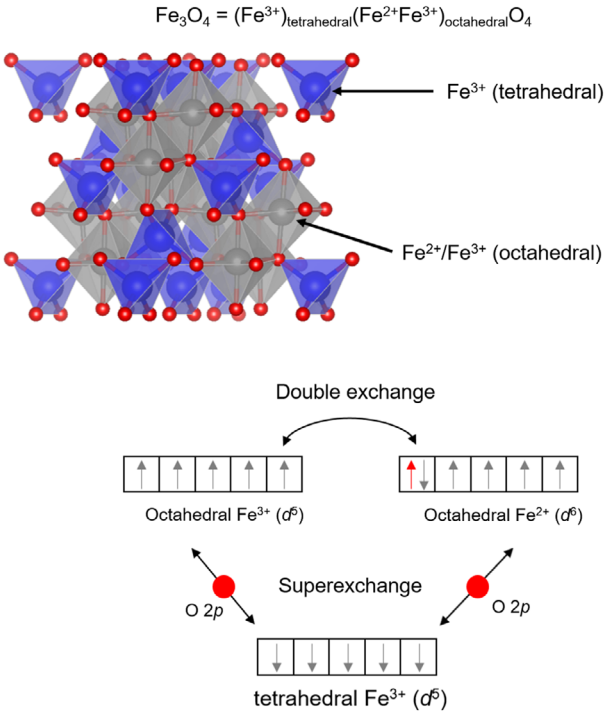

Figure 1. At the top, crystal structure of inverse spinel (Fe_3O_4); Fe^{3+} (blue) and Fe^{2+}/Fe^{3+} (gray) in the tetrahedral and octahedral based on the face-centered-cubic structure of O^{2-} ions (red). At the bottom, electron configuration and the exchange interactions of Fe ions in Fe_3O_4.

decomposition temperature, growth rate, and crystallinity, and purity of the CVD deposit.[16] Bloesser et al. synthesized phase-pure magnesium ferrite by a microwave-assisted method with $Mg(acac)_2$ and $Fe(acac)_3$ precursors and calcination as a post-treatment enabled to control the degree of inversion. The increasing temperature induced particle agglomeration and high degree of inversion. However, further temperature rising resulted in lowering the degree of inversion.[17] Pradhan et al. also synthesized $MgFe_2O_4$ by ball milling of MgO and Fe_2O_3 and controlled the degree of inversion by postannealing. Pradhan et al. found increasing the degree of inversion by confirming increasing occupancy of Fe^{3+} in octahedral site along increasing the post-annealing temperature.[18] In order to obtain phase-pure $NiGa_2O_4$, $[NiGa_2(O^tBu)_8]$ was used in two different CVD configurations. While the normal CVD setup yields mixed phases of $NiGa_2O_4$, Ni, and NiO due to premature decomposition of the Ni–Ga mixed-metal precursor, shortening the reactor length and modifying the precursor flux to maintain a laminar flow and an intact transport of the precursor, single-phase $NiGa_2O_4$ was obtained.[19] Similarly, low-temperature synthesis of nanocrystalline zinc aluminate spinel ($ZnAl_2O_4$) from the molecular precursor, $[ZnAl_2(O^iPr)_8]$, produced partially inverse spinel at a lower temperature (<900 °C, degree of inversion ≈ 0.3), whereas a regular spinel was obtained at 1000 °C.[20] Although the effects of the degree of inversion in spinel ferrites such as magnetic and optical properties are well-known, the methods to control the degree of inversion are less studied and mostly limited to high-pressure studies. For example, the influence of an external magnetic field during spinel synthesis has not been investigated in detail so far.

Our previous studies demonstrated the effect of external magnetic fields on the morphology, phase formation, and catalytic properties of functional materials synthesized by magnetic field-assisted chemical vapor deposition (CVD).[21–25] We report herein on the synthesis of $MgFe_2O_4$ thin film by CVD of a single-source precursor, $[MgFe_2(O^tBu)_8]$, under applied magnetic field and zero-field conditions. The influence of the external magnetic field on structural properties and chemical composition was studied by X-ray diffraction data and X-ray photoelectron spectroscopy (XPS), respectively. The incipient inversion in the spinel structure as a function of the magnetic field was studied by X-ray absorption spectroscopy (XAS) and the X-ray magnetic circular dichroism (XMCD) that confirmed a higher degree of inversion in $MgFe_2O_4$ deposits grown in external magnetic.

2. Results and Discussion

The heterometallic alkoxide precursor $[MgFe_2(O^tBu)_8]$ (**1**) used for the deposition of $MgFe_2O_4$ (MFO) films was synthesized by following a previously reported salt metathesis reaction between $K[Fe(O^tBu)_4]$ and anhydrous magnesium chloride (**Figure 2**).[13,26,27]

The structural motif of **1** resembles the heterometallic spiro compounds of general formula $[M\{M'(O^tBu)_4\}_2]$ (M = Co, Zn, Ni, M' = Fe, Al),[13,16,26–29] exhibiting a bivalent central cation coordinated in a bidentate manner by the two *tert*-butoxo ligands of the tetrahedral $Fe(O^tBu)_4\}^-$ alkoxometallate units (Figure 2).

Thermogravimetric analysis (TG) of **1** (**Figure 3a**) indicated instant hydrolysis of the precursor in the initial phase which is common in metal alkoxides, which demonstrates their intrinsically high reactivity, making them attractive precursors for metal oxides.[30–34] The three-step decomposition led to a total mass loss of 69% (7.327 mg of 10.6189 mg) ($\Delta m_1 = 64\%$ (6.796 mg) in the range 25–260 °C, $\Delta m_2 = 4\%$ (0.425 mg) in the range 260–500 °C, and $\Delta m_3 = 1\%$ (0.106 mg) in the range 500–900 °C) that is close to the theoretical mass loss of 72% expected for the formation of $MgFe_2O_4$. The deviation in the

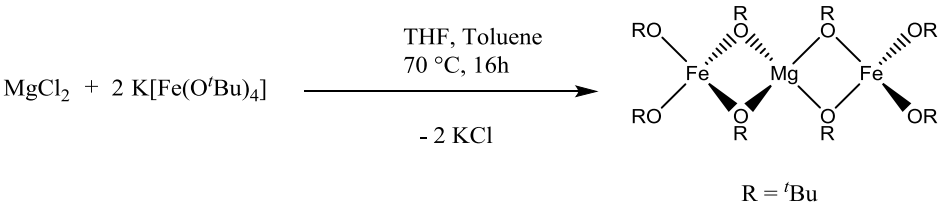

Figure 2. Salt metathesis reaction for the synthesis of heterometallic precursor **1**.

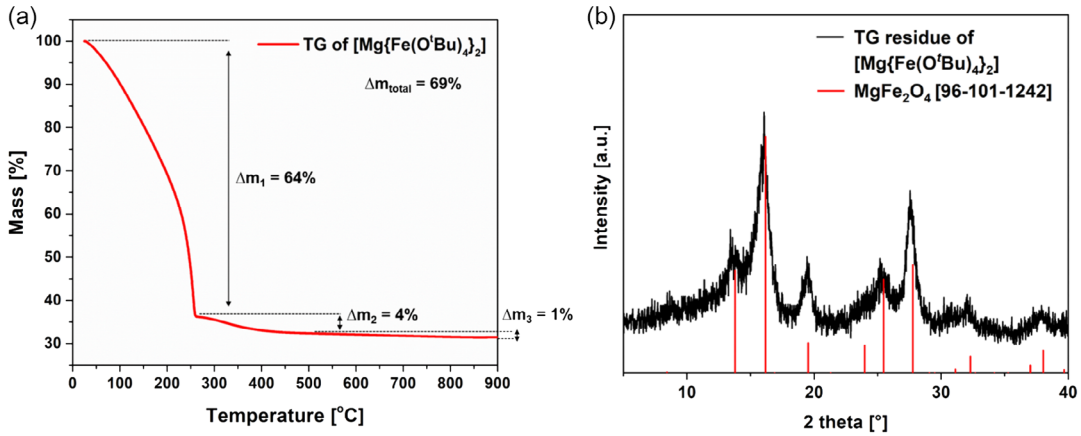

Figure 3. a) Thermogravimetric measurement of [Mg{Fe(O^{t}Bu)$_4$}$_2$] (**1**) up to 900 °C with a heating rate of 10 °C min^{-1} and b) powder X-ray diffraction pattern of the TG residue with literature data shown as red vertical lines (JCPDS #96-101-1242).

weight loss is possible due to the initial hydrolysis, which is inevitable despite the precursor handling in dry nitrogen, of the sample. Alternatively, the deviation from the theoretical value is possible due to the minor losses associated with the vaporization of a tiny fraction of the precursor. Any weight loss at temperatures higher than 500 °C was negligible indicating the formation of a solid of definite composition. Consequently, it was considered suitable as the substrate temperature for CVD. The formation of a solid-state ternary compound ($MgFe_2O_4$) of definite composition was confirmed by powder X-ray diffraction of the solid residue collected from the crucible (Figure 3b).

The $MgFe_2O_4$ films (MFO) were grown in a magnetic field-assisted CVD process using the heterometallic single-source precursor **1** in a cold-walled CVD reactor fit with a perpendicularly aligned permanent magnet. The MFO films were grown on fluorine-doped tin oxide (FTO) by heating the precursor to 180 °C and maintaining the substrate temperature at 500 °C for 20 min. To elucidate the influence of the magnetic field on the growth of MFO film, CVD was performed under both zero-field ($B = 0$) and field-assisted ($B = 0.5$ and 1 T) conditions. The formation of the $MgFe_2O_4$ spinel phase was verified by X-ray diffraction and XPS studies, which confirmed the phase purity and elemental stoichiometry (cubic structure and space group: Fd-3m), respectively (**Figure 4** and **5**). The X-ray diffraction (XRD) pattern (Figure 4c) confirmed the successful deposition of $MgFe_2O_4$ thin films by mfCVD technique, indicating diffraction peaks at 30.01°, 35.46°, 43.14°, and 57.04° corresponding to the (220), (311), (400), and (511) planes following the literature data (JCPDS# 01-088-1938) and indicating the formation of an inverse spinel structure (Figure 4b). Overall, the three $MgFe_2O_4$ thin films grown under different magnetic fields showed similar diffraction patterns and phase structure. However, the (400) peak intensity was found to gradually diminish when the applied magnetic field was increased up to 0.5 T. For comparison, the simulated XRD pattern shows (Figure 4d) a systematic decay of peak intensity for the (400) plane as a function of the degree of inversion of spinel structure, suggesting a magnetic domain reorientation during the mfCVD and consequent inversion of $MgFe_2O_4$ spinel structure. As comparing the measured and simulated XRD patterns, the lowered (400) intensity (Figure 4c) at 0.5 T indicates the high degree of inversion and the increased (400) intensity at 0 and 1.0 T indicates the lowered degree of inversion. This tunable degree of inversion according to the external field matches the X-ray magnetic circular dichroism (XMCD) results below which explain increasing and decreasing magnetic moments indicating the degree of inversion.

The XPS analyses confirmed the presence of magnesium, iron, and oxygen in all three samples with small amounts of carbon originating from residual precursor fragments adhering to the walls of the CVD chamber (Figure 5a). The high-resolution spectra of the Fe 2*p* peak centered at 710.3 eV confirmed that iron is mainly present in the Fe^{3+} valence state as supported by the characteristic satellite feature around 719 eV. Minor traces of Fe^{2+} (708.3 eV) were also found, which is an indication of a field-driven chemical reduction or antisite defects of Fe^{2+} occupying the Mg^{2+} position.[35]

Although no pronounced texturing effects were observed in the XRD characterization data of MFO films deposited under zero-field and field-assisted conditions (Figure 4), the application of an external magnetic field affects the topology of the grains in MFO films, analyzed by dual-beam focused ion beam–scanning electron microscopic analysis (FIB–SEM, **Figure 6**). As-grown films showed a uniform deposition of MFO on FTO substrates, whereas films deposited with an applied magnetic field perpendicular to the precursor flow (Figure 5C and 6B) exhibited larger grain sizes with pronounced grain boundaries when compared to MFO films grown under zero-field conditions (Figure 6A). The magnetic field effects on grain density and crystal size were previously observed; however, the field of magnetic field-assisted CVD remains elusive.[21,34] The surface analysis performed through the image processing software (ImageJ) indicated about 2–3% of surface porosity in MFO films deposited under zero-field conditions, whereas no porous morphology was observed in MFO films grown at 0.5 and 1 T. Cross-sectional analyses of MFO films (Figure 6D–F) did not indicate any specific trend in the film thickness, although MFO films grown at $B = 1$ T showed the highest thickness of 1.91 µm compared to 0 T (Figure 6D, 1.23 µm) and 0.5 T (Figure 6E, 0.88 µm).

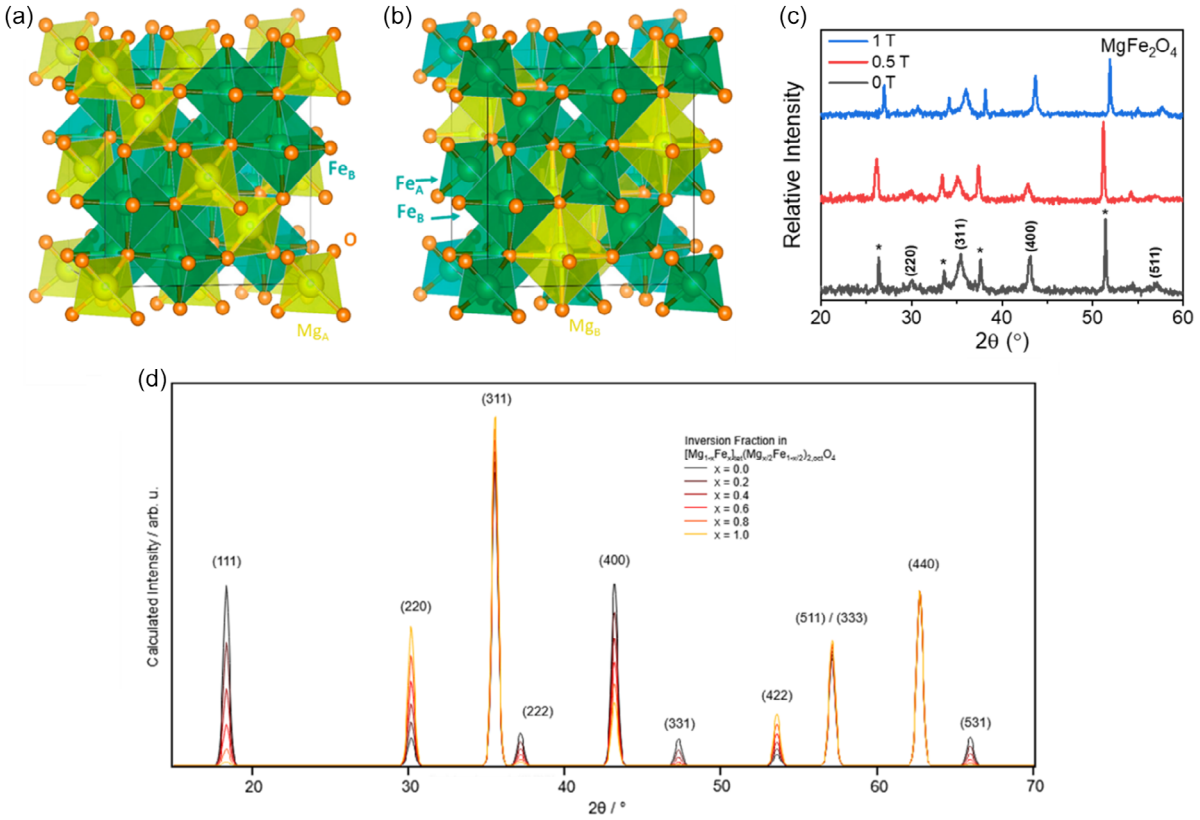

Figure 4. Crystal structure of $MgFe_2O_4$ ferrite a) normal spinel b) inverse spinel, c) XRD pattern of chemical vapor deposited $MgFe_2O_4$ under 0, 0.5, and 1 T magnetic field ($T_{substrate} = 500\,°C$, $T_{precursor} = 180\,°C$, $t_{deposition} = 20$ min). d) Simulated XRD pattern as a function of the degree of inversion.

Figure 7 represents the absorbance spectra of MFO films as a function of the applied magnetic field. MFO-0 T sample absorbed in a wide wavelength range (300–650 nm) and showed the highest absorbance. The decreased absorbance might microscopically be related to the increased grain size of the films deposited under a magnetic field (Figure 6). In the order of thickness, MFO-1.0 T is the thickest, and MFO-0.5 T is the thinnest but in the order of absorbance, MFO-0 T is the highest. Therefore, the thickness effect is excluded and the optical properties enable it to be manipulated by controlling grain size and magnetic field.

From the viewpoint of the local atomic and electronic structure investigated by the XAS, both the Fe-L- and the Mg-K- edges (**Figure 8**a,b) show very little changes with field strength during deposition. The changes in both the white line (maximum) intensity and energy of the Fe L3 edge (Figure 8a) (≈707 eV) could not be compared due to the charging of the samples, which leads to distortion at high-intensity levels. In general, the spectra are quite similar and are in line with a d^5 electronic configuration (indicating Fe^{3+}). The Mg-K-edges (Figure 8b) show similar behavior and apart from a change in absolute intensity in the triplet peak structure around 1300 eV, there is no significant difference visible in the XAS data. The general characteristics of the spectra, which are mostly dictated by the symmetry around the Mg center as there is little deviation from the formal Mg^{2+} to be expected, are most similar to the signature of enstatite and diopside, where Mg resides in octahedral coordination.[36] This suggests that the $MgFe_2O_4$ deposited through mfCVD is spinel with considerable inversion. The variation in inversion fraction with the magnetic field during deposition, which is suggested by changes in the intensity of the (400) peak, is only marginally corroborated here, as the structure of the XAS essentially stays similar. However, the most interesting aspect is the O-K-edge spectra (Figure 8c), which showed a decrease in the pre-edge peak at ≈529 eV in samples deposited under 1 T. This region is related to the octahedral Fe–O environment, where the electronic states make up most of the region of the Fermi level and are of O 2*p* parentage constituted by nonbonding orbitals on O atoms to antibonding t_{2g} orbitals of Fe atoms. The decrease of the prepeak feature, in simple terms, suggests a depletion of charge carries, as the lowest unoccupied molecular orbital (LUMO) that is accessed here is a direct measure of the hole concentration

The lowering in the intensity of the (400) plane as a function of the magnetitic field in XRD suggests that the applied magnetic field critically influenced the crystal facets and triggered a preferential lattice growth in MFO films. Alternatively, the occupancy of Mg and Fe atoms in tetrahedral and octahedral centers defining the degree of inverse spinel structure could be impacted, as such that the suppression of (400) plane (in simulated XRD depicted in Figure 4d) with 0.5 T fields indicating the inversion of structure. In accordance with the XAS results (Figure 8), the UV–vis spectroscopy showed that the MFO-0 T samples absorbed illuminated light in a wider wavelength range that is indicative of a differential amount of Fe^{3+} ions in octahedrally coordinated sites.

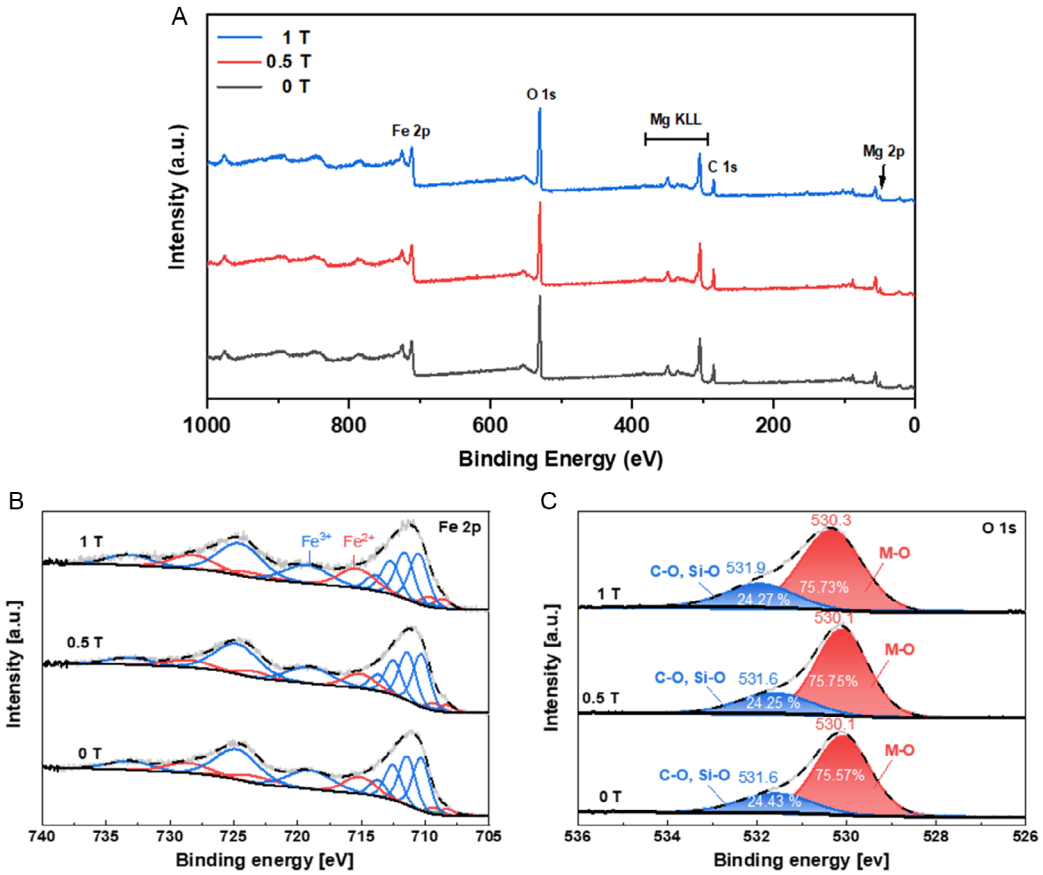

Figure 5. The XPS analytical data representing A) a survey spectrum, B) Fe 2*p*, and C) O 1*s* of deposited MFO films via mfCVD of precursor **1** with different field strength ($B = 0$, 0.5, and 1 T).

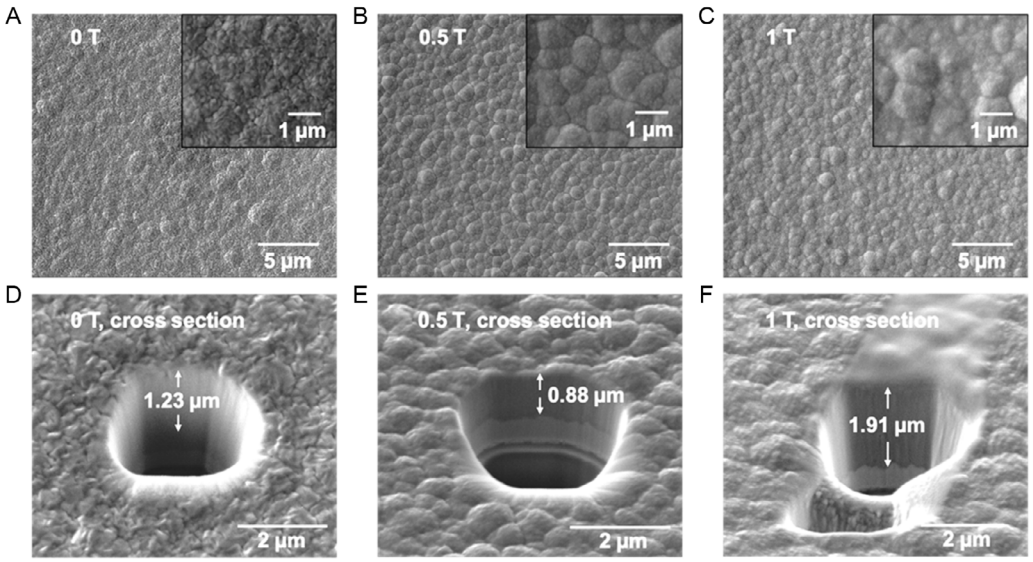

Figure 6. FIB–SEM images of deposited films using precursor **1** in CVD with zero-field A), 0.5 T B), and 1 T C) perpendicular to the precursor flow as well as a cross section of MFO films D: 0 T, E: 0.5 T, and F: 1 T).

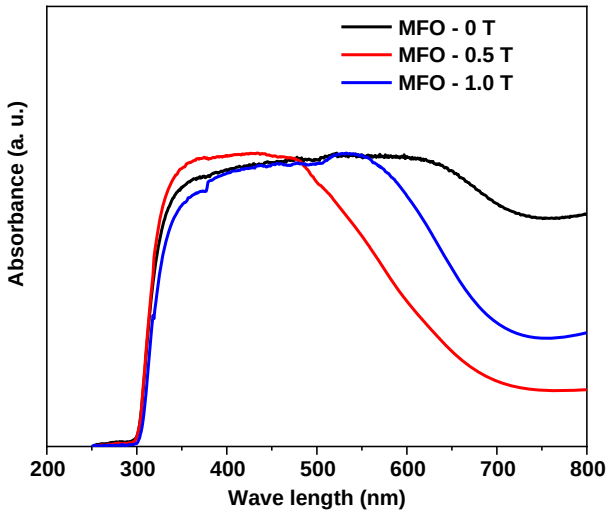

Figure 7. UV–vis absorption spectra of the deposited films.

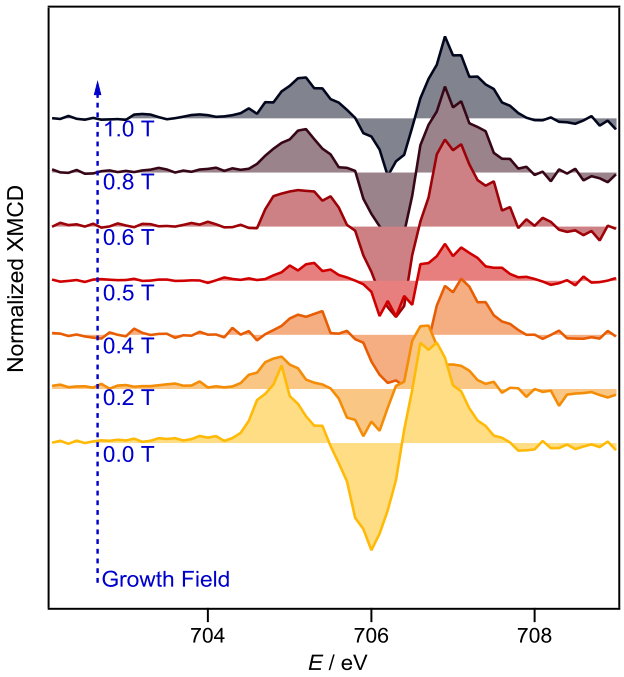

Figure 9. Normalized XMCD spectra of MFO thin films deposited under 0–1 T magnetic fields.

Further, the XMCD measurements were conducted to study the magnetic properties of a specific element, such as its spin and orbital magnetic moment. In the case of the Fe atom present in the spinel structure, a $2p$ electron is excited to a $3d$ state by an X-ray photon of about 700 eV. Because the $3d$ electronic states are the origin of the magnetic properties of the elements, the spectra contain information on their magnetic properties. The XMCD spectra shown in **Figure 9** indicated a decreasing magnetic moment with an increase in the external field applied during the deposition up to 0.5 T. This decrease in the magnetic moment is relevant to the higher degree of inversion in the

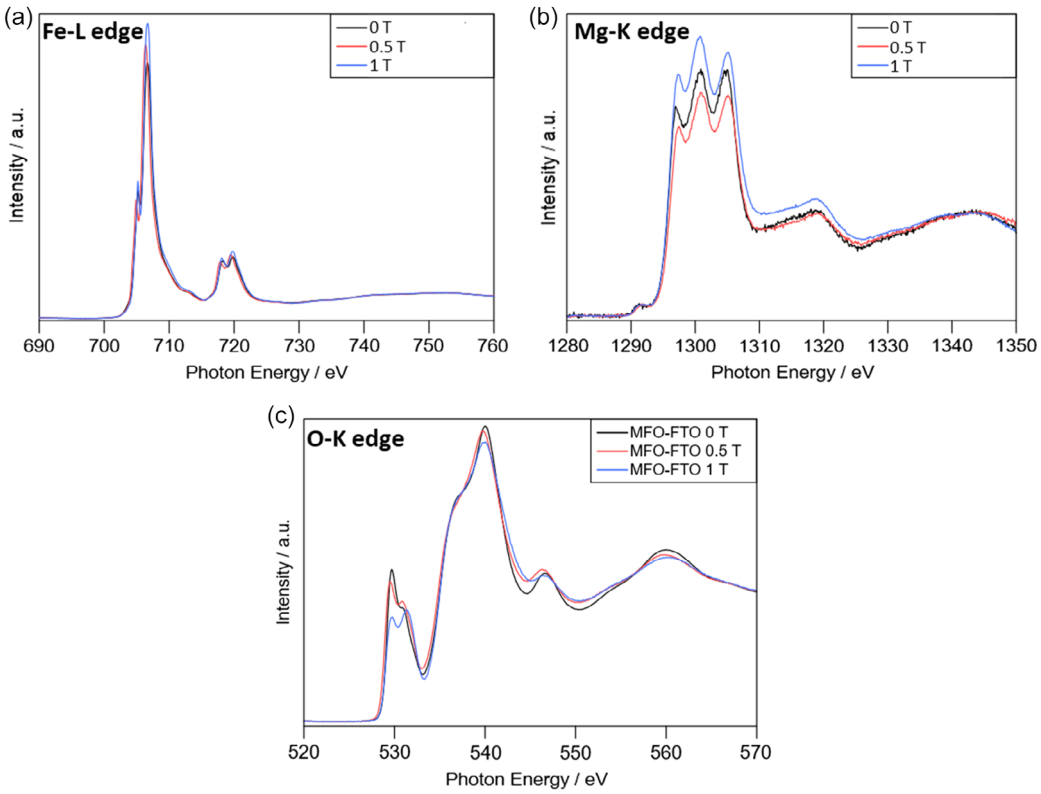

Figure 8. XAS spectra for Fe-L a), Mg-K b), and O-K c) edges of $MgFe_2O_4$ deposited under different magnetic fields.

spinel lattice evident until an applied field of 0.5 T. The XMCD spectra of the samples grown at a higher magnetic field showed higher magnetic moments of the Fe atom. The published data[12,17] suggest, based on Fe L-edge spectra, that the occupancy of octahedral Fe^{3+} differs between the magnetized and reference films, which indicates that magnetization affects the degree of inversion. A plausible explanation for the nonlinear behavior of the influence of field on the degree of inversion in this study appears to be a result of two counterbalancing effects: on the one hand, the applied magnetic field (1 T) influences the film growth (e.g., interaction with precursor flux or with any adsorbates/nucleation intermediates); on the other hand, it is not strong enough to affect the solid state as expected in the case of magnetic annealing. In order to see a magnetic annealing effect, stronger fields might be necessary to overcome ion migration barriers, which were not possible with the current experimental setup.

3. Conclusion

Magnesium ferrite (MFO) films were successfully deposited in a CVD process using a single-source precursor $[Mg\{Fe(O^tBu)_4\}_2]$ under zero-field and magnetic field-enhanced deposition conditions. The external magnetic field applied during the CVD process was found to promote grain growth that influenced the optical properties of samples deposited under zero-field and applied field conditions. Exemplified by the structural data and magnetic dichroism results, CVD under an external magnetic field influences the magnetic domain of the $MgFe_2O_4$ spinel sublattice and inversion of the crystal structure. Compared to compositional modifications such as doping or energy-consuming heat treatment processes, the external magnetic field seems an attractive and reproducible soft parameter to control the degree of inversion, which in turn can substantiate a range of functional properties of spinel ferrites.

4. Experimental Section

Precursor Synthesis: The precursor synthesis was carried out under inert atmosphere (nitrogen gas) using a *Stock* glass vacuum line. All used reagents were used without further purification and the solvents were freshly distilled over sodium. TG analysis was performed by a TG/DSC1 (Mettler Toledo GmbH, Germany) apparatus using nitrogen gas and a heating rate of 10 °C min^{-1}.

$[Fe(O^tBu)_3]_2$: A suspension of anhydrous $FeCl_3$ (5.78 g, 36 mmol) in dry toluene (50 mL) was cooled using liquid nitrogen and dry THF (150 mL) was slowly added. After the mixture thawed, a solution of fresh sublimed KO^tBu (12.09 g, 108 mmol) in dry THF (150 mL) was added and the suspension was stirred for 24 h at 80 °C. The solvent was removed under reduced pressure and the product was obtained after sublimation at 90 °C in vacuo ($p = 10^{-2}$ mbar) as a green solid, yielding 7.15 g (26 mmol, 72%). Molar mass: 550.38 g mol^{-1}; Found C, 51.8; H 9.2. Calc. C, 52.4; H, 9.8%.

$[Mg\{Fe(O^tBu)_4\}_2]$ (1): For the synthesis of $[Mg\{Fe(O^tBu)_4\}_2]$, KO^tBu (2.0 eq) in dry THF (25 mL) was added to a solution of $[Fe(O^tBu)_3]_2$ (1.23 g, 2.24 mmol) in 40 mL toluene. Afterward, anhydrous $MgCl_2$ (0.11 g, 1.12 mmol) in 25 mL dry THF was added and the reaction was stirred overnight at 70 °C. The formed KCl was removed by extraction with pentane (2 × 15 mL) and the product was obtained as a green–yellow solid by sublimation ($T_{sublimation} = 140$ °C, $p = 10^{-2}$ mbar). Molar mass: 720.38 g mol^{-1}.

MfCVD Deposition: For the deposition of MFO films a cold-walled system, an external horizontal magnetic field (2 × 2 cm^2, DC current), produced by an electromagnet (MagMess EM- 2), was used. FTO substrates (1 × 1.5 cm) were heated to 500 °C using a DC Joule heater and 100 mg of the precursor in a 10 mL flask was implemented by a glass flange into the system. The deposition was performed by a precursor temperature of 180 °C and a deposition time of 20 min.

Physicochemical Characterization: The X-ray diffraction characterization of the synthesized powders and films was measured on a STOE diffractometer with STADI MP system (Cu Kα = 1.54178 Å, 40 kV, 40 mA). FIB–SEM images of MFO films were measured using a Strata Dual Beam 235 from FEI. Chemical analysis of the surfaces was performed using XPS utilizing an ESCA M-Probe spectrometer from Surface Science Instruments (SSI), which is equipped with a monochromatic Al Kα (1486.6 eV) X-ray source. All recorded spectra were referent to a binding energy of 284.8 eV based on the C 1*s* signal from adventitious carbon. Compositional calculations were performed using CasaXPS. XAS and XMCD were recorded with synchrotron radiation (BESSY-II, HZB) and normalized typically with the two-point method (at the far-lowest and highest-energy points of each edge).

Acknowledgements

The presented work was funded by the framework of the priority program SPP1959 of the *Deutsche Forschungsgemeinschaft (DFG)*. The authors gratefully thank the University of Cologne and the Excellence Cluster "Quantum Matter and Materials" for infrastructural support. The authors also acknowledge the support of Mr. Dirk Pullem (Elemental Analysis). X-ray absorption spectroscopy and X-ray magnetic circular dichroism measurements were carried out at the UE56-1_SGM beamline at the BESSY II electron storage ring operated by the Helmholtz–Zentrum Berlin für Materialien und Energie, which is thankfully acknowledged.

Open Access funding enabled and organized by Projekt DEAL.

Conflict of Interest

The authors declare no conflict of interest.

Data Availability Statement

The data that support the findings of this study are available from the corresponding author upon reasonable request.

Keywords

chemical vapor deposition, heterometallic alkoxides, magnesium ferrite, magnetic field, single-source precursor

Received: January 4, 2023
Revised: April 20, 2023
Published online: June 14, 2023

[1] A. Goldman, *Mod. Ferrite Technol.* **2006**, 220.
[2] M. Sugimoto, *J. Am. Ceram. Soc.* **1999**, *82*, 269.
[3] M. Azam, M. A. Zeeshan, S. Riaz, S. Naseem, *Mater. Today: Proc.* **2015**, *2*, 5705.
[4] E. J. W. Verwey, E. L. Heilmann, *J. Chem. Phys.* **1947**, *15*, 174.
[5] V. Šepelák, K. Tkáčová, V. V. Boldyrev, S. Wißmann, K. D. Becker, *Phys. B Condens. Matter* **1997**, *234–236*, 617.
[6] N. Aliyan, S. M. Mirkazemi, S. M. Masoudpanah, S. Akbari, *Appl. Phys. A Mater. Sci. Process.* **2017**, *123*, 446.

[7] X. Zeng, J. Zhang, S. Zhu, X. Deng, H. Ma, J. Zhang, Q. Zhang, P. Li, D. Xue, N. J. Mellors, X. Zhang, Y. Peng, *Nanoscale* **2017**, *9*, 7493.
[8] L. Zhou, J. Liu, A. Lu, J. Shen, J. Xu, H. Jiang, *Chem. Eng. J.* **2022**, *428*, 131174.
[9] S. Wang, D. Li, C. Yang, G. Sun, J. Zhang, Y. Xia, C. Xie, G. Yang, M. Zhou, W. Liu, *J. Sol-Gel Sci. Technol.* **2017**, *84*, 169.
[10] N. Sivakumar, S. R. P. Gnanakan, K. Karthikeyan, S. Amaresh, W. S. Yoon, G. J. Park, Y. S. Lee, *J. Alloys Compd.* **2011**, *509*, 7038.
[11] E. K. Fodjo, K. M. Gabriel, B. Y. Serge, D. Li, C. Kong, A. Trokourey, *Chem. Cent. J.* **2017**, *11*, 58.
[12] T. S. Herng, W. Xiao, S. M. Poh, F. He, R. Sutarto, X. Zhu, R. Li, X. Yin, C. Diao, Y. Yang, X. Huang, X. Yu, Y. P. Feng, A. Rusydi, J. Ding, *Nano Res.* **2015**, *8*, 2935.
[13] S. Mathur, C. Cavelius, H. Shen, *Z. Anorg. Allg. Chem.* **2009**, *635*, 2106.
[14] T. Lehnen, D. Zopes, S. Mathur, *J. Mater. Chem.* **2012**, *22*, 17732.
[15] M. Büyükyazi, C. Hegemann, T. Lehnen, W. Tyrra, S. Mathur, *Inorg. Chem.* **2014**, *53*, 10928.
[16] S. Mathur, M. Veith, T. Ruegamer, E. Hemmer, H. Shen, *Chem. Mater.* **2004**, *16*, 1304.
[17] A. Bloesser, H. Kurz, J. Timm, F. Wittkamp, C. Simon, S. Hayama, B. Weber, U. P. Apfel, R. Marschall, *ACS Appl. Nano Mater.* **2020**, *3*, 11587.
[18] S. K. Pradhan, S. Sain, H. Dutta, *ISRN Ceram.* **2011**, *2011*, article no. 194575, https://doi.org/10.5402/2011/194575.
[19] S. Mathur, S. Barth, H. Shen, *Chem. Vap. Depos.* **2005**, *11*, 11.
[20] S. Mathur, M. Veith, M. Haas, H. Shen, N. Lecerf, V. Huch, S. Hüfner, R. Haberkorn, H. P. Beck, M. Jilavi, *J. Am. Ceram. Soc.* **2001**, *84*, 1921.
[21] A. Raauf, J. Leduc, M. Frank, D. Stadler, D. Graf, M. Wilhelm, M. Grosch, S. Mathur, *Inorg. Chem.* **2021**, *60*, 1915.
[22] M. Pyeon, V. Rauch, D. Stadler, M. Gürsoy, M. Deo, Y. Gönüllü, T. Fischer, T. Hwang, S. Mathur, *Adv. Eng. Mater.* **2019**, *21*, 1900195.
[23] D. Stadler, T. Brede, D. Schwarzbach, F. Maccari, T. Fischer, O. Gutfleisch, C. A. Volkert, S. Mathur, *Nanoscale Adv.* **2019**, *1*, 4290.
[24] D. Stadler, D. N. Mueller, T. Brede, T. Duchoň, T. Fischer, A. Sarkar, M. Giesen, C. M. Schneider, C. A. Volkert, S. Mathur, *J. Phys. Chem. Lett.* **2019**, *10*, 6253.
[25] M. Frank, L. Ju, J. Leduc, D. Stadler, D. Graf, I. Gessner, F. Zajusch, T. Fischer, M. Rose, D. N. Mueller, S. Mathur, *Inorg. Chem.* **2019**, *58*, 10408.
[26] M. Veith, M. Haas, V. Huch, *Chem. Mater.* **2005**, *17*, 95.
[27] C. Gatel, B. Warot-Fonrose, S. Matzen, J. B. Moussy, *Appl. Phys. Lett.* **2013**, *103*, 092405.
[28] S. Mathur, C. Cavelius, K. Moh, H. Shen, J. Bauer, *Z. Anorg. Allg. Chem.* **2009**, *635*, 898.
[29] F. Meyer, A. Dierstein, C. Beck, W. Härtl, R. Hempelmann, S. Mathur, M. Veith, *Nanostruct. Mater.* **1999**, *12*, 71.
[30] V. Nahrstedt, D. Stadler, T. Fischer, T. Duchoň, D. N. Mueller, C. M. Schneider, S. Mathur, *Inorg. Chem.* **2021**, *60*, 3719.
[31] A. Jamil, J. Schläfer, Y. Gönüllü, A. Lepcha, S. Mathur, *Cryst. Growth Des.* **2016**, *16*, 5260.
[32] H. Lu, D. S. Wright, S. D. Pike, *Chem. Commun.* **2020**, *56*, 854.
[33] M. Catauro, I. Blanco, D. Naviglio, G. D. Poggetto, *Macromol. Symp.* **2021**, *395*, 2000197.
[34] J. Sun, Q. B. Wen, T. Li, L. Wiehl, C. Fasel, Y. Feng, D. De Carolis, Z. J. Yu, Q. G. Fu, R. Riedel, *J. Am. Ceram. Soc.* **2020**, *103*, 1436.
[35] M. C. Biesinger, B. P. Payne, A. P. Grosvenor, L. W. M. Lau, A. R. Gerson, R. S. C. Smart, *Appl. Surf. Sci.* **2011**, *257*, 2717.
[36] N. Trcera, D. Cabaret, S. Rossano, F. Farges, A. M. Flank, P. Lagarde, *Phys. Chem. Miner.* **2009**, *36*, 241.